Journal of Electron Spectroscopy and Related Phenomena 233 (2019) 64–68

Contents lists available at ScienceDirect

Journal of Electron Spectroscopy and Related Phenomena

journal homepage: www.elsevier.com/locate/elspec

Operando measurement of single crystalline $Li_4Ti_5O_{12}$ with octahedral-like morphology by microscopic X-ray photoelectron spectroscopy

Keishi Akada[a,b], Takaaki Sudayama[b], Daisuke Asakura[b,c], Hirokazu Kitaura[b], Naoka Nagamura[d,e], Koji Horiba[f], Masaharu Oshima[g], Eiji Hosono[b,c,*], Yoshihisa Harada[a,c,g,*]

[a] *Institute for Solid State Physics, The University of Tokyo, Kashiwa, Chiba 277-8581, Japan*
[b] *Research Institute for Energy Conservation, National Institute of Advanced Industrial Science and Technology, Tsukuba, Ibaraki, 305-8568, Japan*
[c] *AIST-UTokyo Advanced Operando-Measurement Technology Open Innovation Laboratory (OPERANDO-OIL), National Institute of Advanced Industrial Science and Technology (AIST), Kashiwa, Chiba, 277-8565, Japan*
[d] *Research Center for Advanced Measurement and Characterization, National Institute for Materials Science, 1-2-1, Sengen, Tsukuba, Ibaraki, 305-0047, Japan*
[e] *PRESTO, Japan Science and Technology Agency, 4-1-8, Honcho, Kawaguchi, Saitama, 332-0012, Japan*
[f] *Institute of Materials Structure Science, High Energy Accelerator Research Organization (KEK), 1-1 Oho, Tsukuba, 305-0801, Japan*
[g] *Synchrotron Radiation Research Organization, The University of Tokyo, Bunkyo-ku, Tokyo, 113-8586, Japan*

ARTICLE INFO

Keywords:
Operando measurement
Microscopic X-ray photoelectron spectroscopy
All-solid-state Li ion battery
$Li_4Ti_5O_{12}$

ABSTRACT

To develop innovative materials for lithium-ion batteries (LIBs), intensive research has been carried out in the research fields of materials, processing, and electrochemistry. Studies of novel analytical methods using synchrotron radiation X-rays have been a focus because understanding the charge-discharge mechanism of LIBs will lead to design strategies for innovative materials. Especially, the establishment of an *operando* measurement system is one of the most important topics to extract the true information of materials, like electronic structures, under the operating conditions as LIBs. We report *operando* microscopic photoelectron X-ray photoemission spectroscopy for octahedral single crystalline $Li_4Ti_5O_{12}$ as an anode material of LIB under the potential control by an all solid-state LIB. From the photoelectron mapping of a single crystal, we confirm the reversible change of Ti 3*p* spectra from a facet of a single crystal at a selected nano-area by Li insertion and extraction.

1. Introduction

Lithium-ion batteries (LIBs) are used not only for electric vehicles, but also as a standard for power generation for renewable energy. In the research and development of LIBs, a strategic design policy of active materials has been inevitable to match the demands for high energy density, high power, cycle performance, and safety from various kinds of users [1]. Simultaneously, analytical techniques for LIBs have become sophisticated to obtain and understand the basic chemical/physical properties of the active materials, such as atomic position, crystal structure, electronic structure, and surface condition [2–11]. These analyses at the early stage were performed at the *ex situ* condition, where the electrodes including the active materials to be investigated were extracted from battery cells at each operating condition, or at the *in situ* condition, where the same environment as the working condition was simulated [12–14]. However, recently it has been found that *ex situ* or *in situ* conditions do not necessarily provide the actual crystal structure or electronic state of LIB materials under operation. *Operando* measurements, where LIB materials are analyzed while under the operating condition, such as the redox reaction by lithium insertion and extraction, have been recognized as an important analytical tool for LIB materials [12–15]. Many researchers have reported various kinds of *operando* measurements for LIB materials. Among their analyses, synchrotron radiation X-rays have been a key probe. For example, hard X-rays have been used for X-ray diffraction (XRD) measurements to investigate the crystal structure [6,12] and for X-ray absorption spectroscopy (XAS) to monitor the oxidation state of transition metals [16,17] Soft X-rays ($\lesssim$2000 eV) have been used for electron spectroscopy, including XAS and photoelectron spectroscopy, to further clarify the electronic structure with high spatial and/or energy resolution, and element/orbital selectivity. [4,5,15,18–20] Previously, we reported an *operando* soft X-ray photoelectron microscopy system, 3DnanoESCA [21–24] installed at University-of-Tokyo Synchrotron Radiation Outstation beamline BL07LSU in SPring-8. This measurement system is

* Corresponding authors at: AIST-UTokyo Advanced Operando-Measurement Technology Open Innovation Laboratory (OPERANDO-OIL), National Institute of Advanced Industrial Science and Technology (AIST), Kashiwa, Chiba, 277-8565, Japan.
E-mail addresses: e-hosono@aist.go.jp (E. Hosono), harada@issp.u-tokyo.ac.jp (Y. Harada).

https://doi.org/10.1016/j.elspec.2019.03.006
Received 2 December 2018; Received in revised form 18 February 2019; Accepted 17 March 2019
Available online 18 March 2019
0368-2048/

suitable for *operando* analysis of the redox reaction during Li insertion/extraction by all-solid-state LIBs using single crystalline $LiCoO_2$ hexagonal plates as active materials [25]. We have successfully analyzed the photoelectron images of the integrated Co 3*p* peak and its spectral profile at a selected area, which demonstrates the usefulness of *operando* analysis.

Herein, we report *operando* analysis of $Li_4Ti_5O_{12}$ (LTO) as an anode material of LIBs by using the 3DnanoESCA station. Graphite, which is one of the most frequently used anode materials in commercially available LIBs, is now a safety concern at low temperature because the high rate of charge/discharge at low temperature causes lithium plating on a graphite anode [26,27]. In contrast, LTO does not cause Li-plating [28,29]and shows good performance against rapid charge/discharge and good cycle stability [29–31]. During charge/discharge of LTO, lithium insertion and extraction proceeds between two co-existing phases, spinel $Li_4Ti_5O_{12}$ and rock salt $Li_7Ti_5O_{12}$ (Li-rich phase) [29]. Nanometer scale analyses of their dynamics have been reported by using transmission electron microscopy (TEM) and electron energy loss spectroscopy (EELS) [32–34]. In this paper, we performed micrometer scale photoemission microspectroscopy analysis at the domain wall of the two phases at the several hundred nanometer resolution, which can selectively analyze each facet surface owing to the surface sensitivity of XPS.

2. Experimental

Single crystalline LTO was fabricated by a flux method. LiCl (3.0 g), Li_2CO_3 (0.0075 mol), and TiO_2 (0.01875 mol) were placed into an Al_2O_3 crucible with a lid. The crucible was placed into a muffle furnace and heated at 1000 °C for 5 h in air. Finally, the samples were washed with deionized water and dried under vacuum condition.

LTO, super P Li as electro-conductive additive, and *N*-methyl-2-pyrrolidone were mixed by sonication to prepare a slurry. The slurry was dropped and dried on the Cu mesh with a carbon coated microgrid, which was connected to a Cu current collector. Then, very thin carbon was coated on the detection side of the Cu mesh. The electrode was used as a working electrode of the *operando* cell. The prepared *operando* cell was set on the five-terminal folder, as shown in Fig. 2. Preparation of the cell and setting on the folder were conducted in an Ar-filled glovebox and this was transferred into the 3DnanoESCA station by a transfer vessel without air exposure. A-B, C and D terminals of the holder were used for the ceramics heater, counter/reference electrode and working electrode, respectively.

For removing water in the dry polymer (polyethylene oxide (PEO)-LiTFSI) of the *operando* cell, the cell was heated at around 55 °C for over 8 h in the high vacuum chamber of the 3DnanoESCA station. After that, the temperature was changed to 50 °C and heating was conducted during measurement to increase of ionic conductivity of both the solid-state electrolytes of LLZ and dry polymer.

For photoelectron microspectroscopy measurement on the 3DnanoESCA station at the BL07LSU beamline in SPring-8, an incident X-ray (1000 eV) was focused by a Fresnel zone plate and order-sorting pinhole aperture of 80 μm was used. Photoelectrons were detected by a modified angle-resolved photoelectron spectrometer (VG Scienta R3000-EWAL) with a pass energy of 200 eV.

During the measurements, terminal C (counter/reference electrode of Li metal) and terminal D (working electrode of LTO) were connected to a potentiostat-galvanostat (solartron 1287) for the electrochemical measurement, and the initial condition was measured under an open-circuit voltage (OCV) condition.

The mapping image from scanning photoelectron microscopy was obtained by the O 1*s* core level spectrum. Selected specific micro-area photoelectron spectra of Ti 2*p* and 3*p* were measured at the initial condition, and after discharge and charge based on this O 1*s* mapping image.

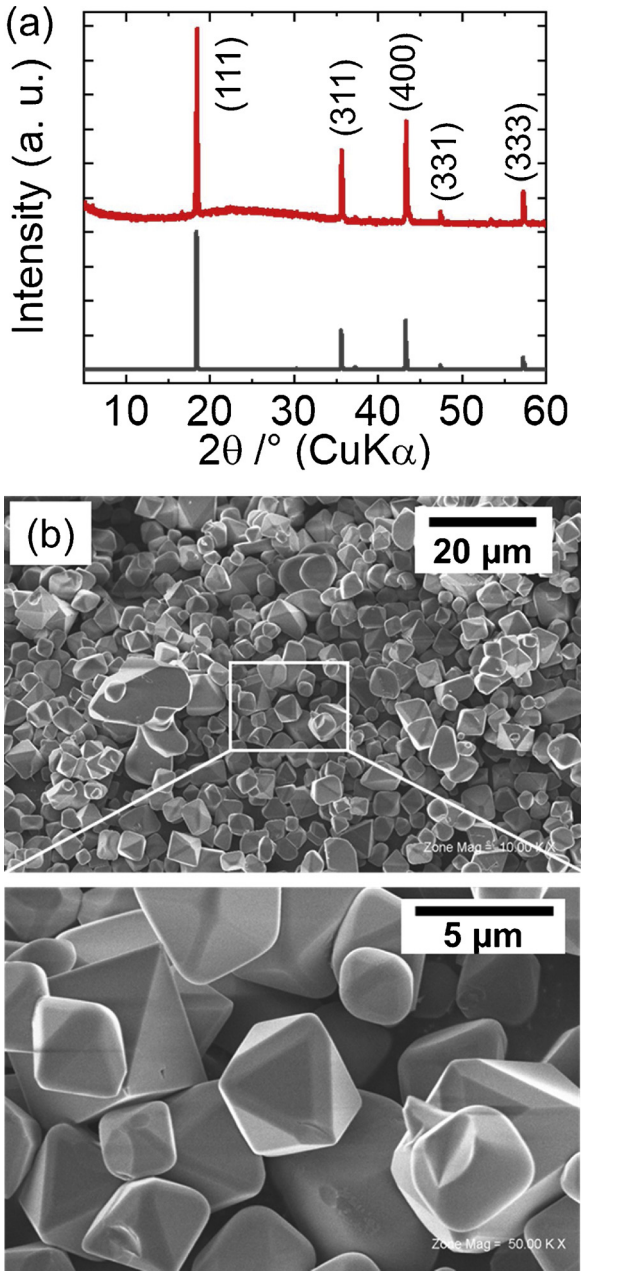

Fig. 1. (a) XRD and (b) SEM images of single crystalline LTO particles.

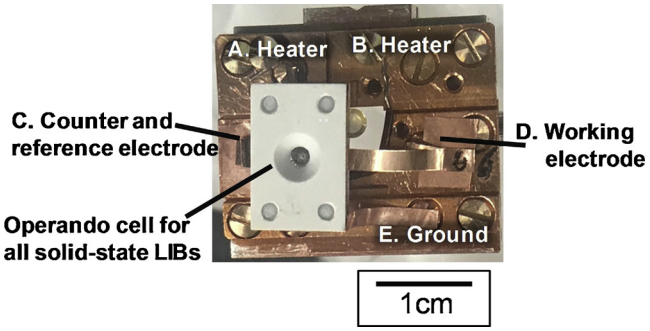

Fig. 2. *Operando* cell system mounted on a sample holder with five terminals.

3. Results and discussion

Fig. 1(a) shows the XRD pattern of LTO samples obtained by a flux method. The XRD pattern was consistent with the simulated pattern from the CIF file 1001098 in the Crystallography Open Database [35]. The lattice constant was calculated to be 8.352 Å, which is similar to the reported value of 8.357 Å, and the symmetry group was Fd-3m:1. SEM images exhibited octahedral particles with triangle facets, as shown in Fig. 1(b). The size of the flat triangle facet was suitable for the mapping of XPS, according to the spatial resolution of the 3DnanoESCA station, because the purpose of the analysis was to understand the mobile domain-wall by the Li-rich and poor phases, which were caused by the valence change of Ti^{4+} and Ti^{3+} related to Li insertion and extraction. For actual *operando* XPS measurements with charge-discharge of LIBs, single crystalline LTO particles with a size of over 5 μm were used as active materials.

Fig. 2 shows an *operando* cell mounted on a sample holder with five terminals. Details of the *operando* cell assembly are described elsewhere [25]. An LTO slurry was dropped and dried on a gold mesh with a carbon-coated micro-grid, which was connected to the Cu current collector to form a working electrode. The working electrode with LTO was coated by a very thin carbon layer to avoid charging of the pure LTO surface owing to the low electrical conductivity of LTO. This was because a noticeable charging was observed in our test XPS measurements using an X-ray tube. From the counter/reference electrode to the working electrode, the Cu current collector, lithium metal, PEO/LiTFSI solid (dry polymer) electrolyte, ceramics electrolyte $Li_7La_3Zr_2O_{12}$ (LLZ), dry polymer and Cu mesh with LTO were all fixed by ceramics jigs. The *operando* cell was set on a ceramics heater to improve the ionic conductivity of the dry polymer and LLZ to accelerate the Li insertion and extraction. Two terminals were used for heating and the other two were used for the working and counter/reference electrodes.

Fig. 3(a) shows a CV curve of the single crystalline LTO having reduction and oxidation peaks by Li insertion and extraction. While, sharp redox peaks of LTO are found around 1.5 V in general [28], a discharge (Li insertion) and a charge (Li extraction) peaks on Fig. 3(a) are centered at 1.0 and 2.2 V, respectively. For the present CV curves, a large overpotential of *operando* cell causes the peak shift with separation of discharge and charge peaks and the peak broadening. After sweeping down to 1.0 V and up to 3.0 V, *operando* XPS measurements were conducted under potentiostatic and OCV conditions; the potentiostatic condition was set at 1.0 V (or 3.0 V) for 3 s and OCV condition for 57 s, which was repeated 300 times. Measurement was started after the first 20 repeating cycles of potentiostatic for 3 s and OCV for 57 s, while waiting for the potential stabilization after the completion of the delayed lithium insertion and extraction because the sweep rate of 0.5 mV/sec was high, owing to the limited measurement time by the synchrotron radiation center. Fig. 3(b) shows OCV curves after the potentiostatic mode at 1.0 V and 3.0 V for 3 s after charge and discharge, respectively. After the potential control at 1.0 V, the potential moves to around 1.5 V. In the two-phase reaction where $Li_4Ti_5O_{12}$ and $Li_7Ti_5O_{12}$ phases coexist, the potential is not changed up to finishing the coexisting state. This imperfect Li insertion results in the small peaks of Ti 3*p* component in Fig. 5(c). After the potential control at 3 V, the potential after 20 repeating cycles is around 2 V. The potential after 100 repeating cycles is over 2.5 V. It is considered that large portion of *operando* measurement is conducted under Li extracted condition.

Fig. 4(a) shows the optical microscope images, and Fig. 4(b) shows O 1*s* (around 450–470 eV) photoelectron mapping images obtained by the 3DnanoESCA station. Furthermore, Fig. 4(c) shows the SEM images observed after the photoelectron mapping from low magnification to high magnification. When the optical image was observed, the in plane XY position of the sample was also recorded. As shown in Fig. 4, similar areas of optical and photoelectron mapping images in low magnification images of Fig.4(a-1), (b-1) and images of selected area of Fig.4(a-2), (b-2) are observed. In high magnification images of Fig.4(a-3,4) and (b-3,4), optical and photoelectron mapping images of the same particles were obtained. These high magnification photoelectron mapping images were obtained after electrochemical operation. Each particle image exhibited a single crystalline LTO. Fig. 4(b-3) shows the octahedral-like morphology of the crystalline LTO. From the SEM image in Fig. 4, similar low magnification and selected area images are observed. In Fig. 4(c-3,4) after the *operando* XPS measurement, the octahedral-like morphology was conserved. The concave-convex shape of the sample surface was clearly observed in the photoelectron mapping owing to the narrow angle of 60 ° formed by the incident beam and the XPS detector.

Pin-point XPS spectra have been measured at the marked points in particles A and B as shown in Fig. 4 under initial open circuit voltage condition, after discharging (Li insertion) and charging (Li extraction). The energy calibration of the XPS spectra in Fig. 5 was performed by setting the Ti 2*p* and 3*p* peaks to 459.3 eV and 37.5 eV in TiO_2 as standards, respectively [36]. As shown in Fig. 5(b), particle A shows much stronger intensity of Li 1*s* [37] than that of Ti 3*s*, while Ti 3*p* intensity for particle B is much stronger than those of Li 1*s* and F 2*s*. It should be also noted that intensity of Ti 3*p* in particle A decreased by discharging (Li insertion). These results suggest that particle A may be covered by Li-F composite overlayer derived from formation of solid electrolyte interface (SEI) by electrochemical reaction between the LTO surface and polymer electrolyte of PEO-LiTFSI. On the other hand, particle B shows almost no SEI formation, suggesting a possibility that this particle may be electrochemically inactive. Fig. 5(c) shows expanded Ti 3*p* spectra of particle A where Ti 3*p* spectra are deconvoluted into two components, Ti^{4+} and Ti^{3+} [38] for the initial condition, Li insertion and Li extraction. The Li-inserted particle shows a small Ti^{3+} component as a shoulder peak in addition to the Ti^{4+} rich component, while the Ti^{3+} component is not observed at all for the initial and Li-extracted samples of particle A. These changes in the Ti 3*p* XPS by the Li insertion and extraction could be understood by considering the nominal valence for each state; three Ti^{4+} sites in the initial $Li_4Ti_5O_{12}$ were reduced to Ti^{3+} by the Li insertion to form $Li_7Ti_5O_{12}$, which resulted in

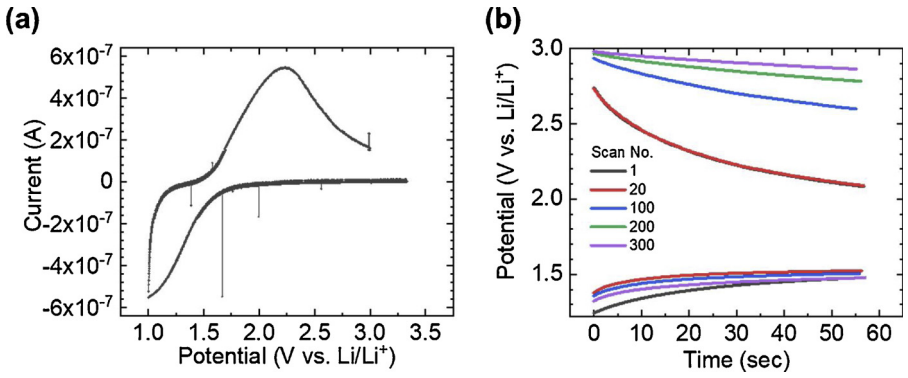

Fig. 3. CV and OCV curves of single crystalline LTO using the *operando* cell assembly.

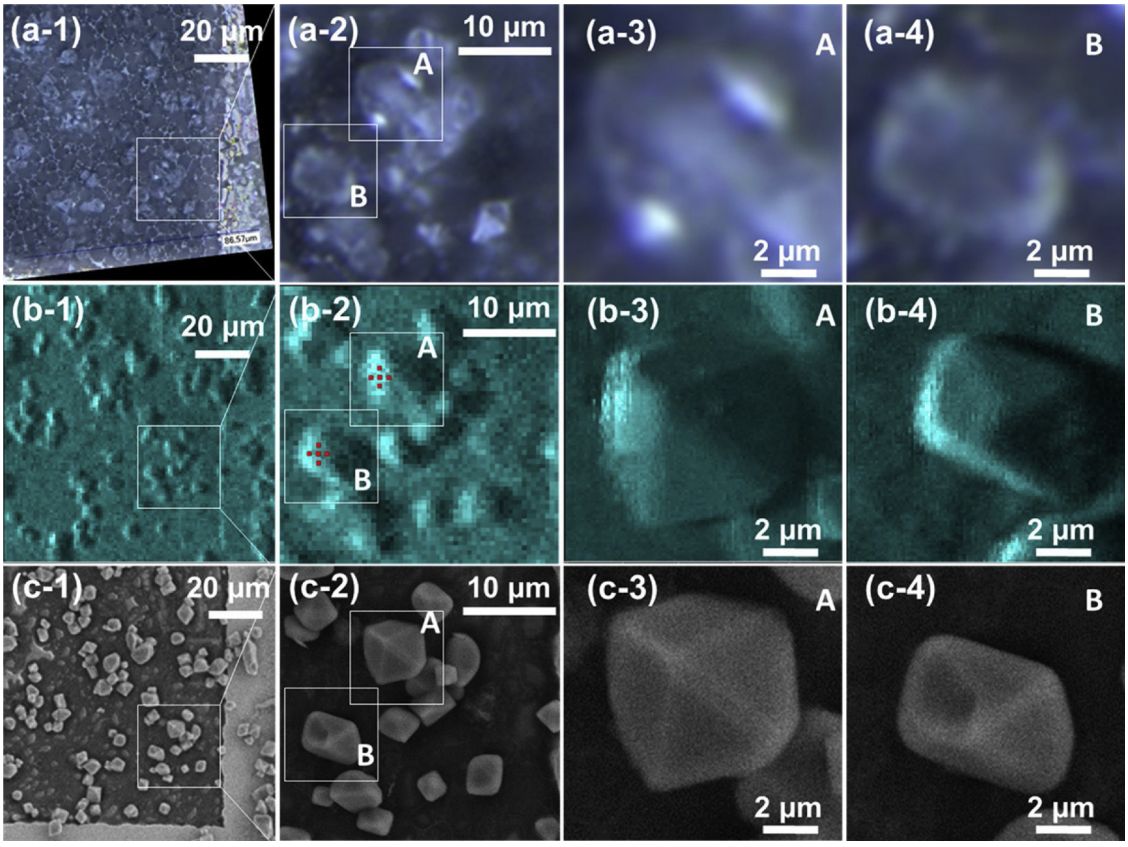

Fig. 4. 2D Optical microscope images (a), photoelectron mapping images (b), and SEM images (c).

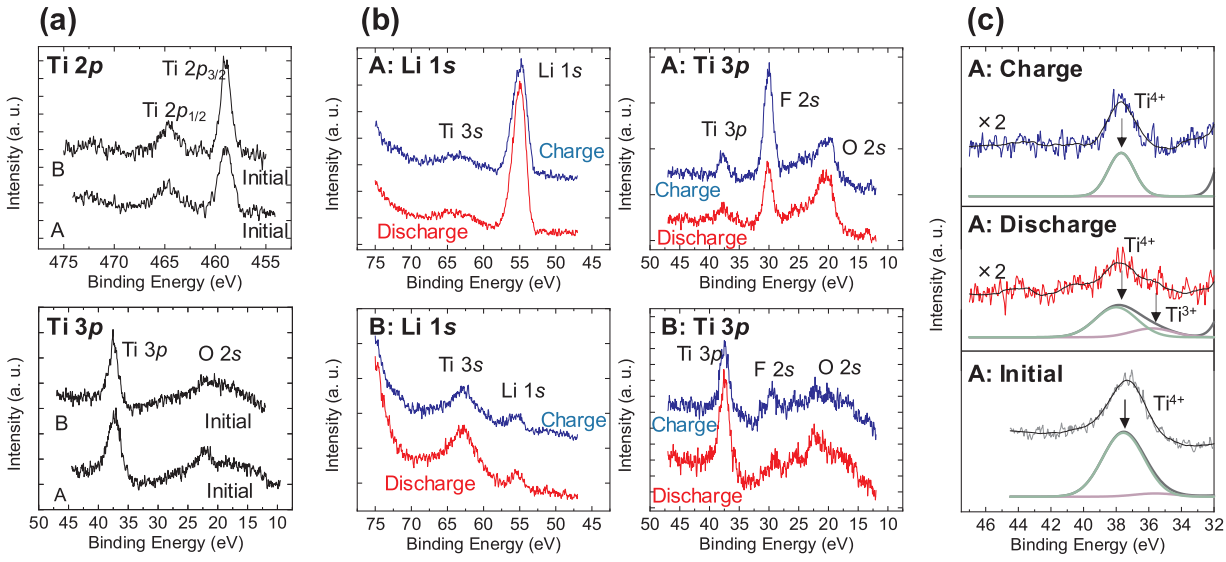

Fig. 5. (a) Ti 2*p* and Ti 3*p* photoelectron spectra under initial open circuit voltage condition of particle A and B. (b) Li 1*s* and Ti 3*p* XPS photoelectron spectra after charge and discharge of particle A and B. (c) Expanded Ti 3*p* peaks of particle A under (a) initial open circuit voltage, discharged and charged condition.

two Ti^{4+} sites and three Ti^{3+} sites. The partial reduction reaction of the Ti site caused appearance of the Ti^{3+} component and a broadening of the Ti 3*p* peaks [38]. In contrast, Ti 3*p* spectra remain almost unchanged for particle B, which is also an evidence for the inactiveness of particle B. Thus microspectroscopy for *operando* analysis of LIBs can provide quite unique information about chemical properties of micrometer scale individual particles.

In this paper, peak changes in the Ti 3*p* spectra were observed at the selected facet. The measurement of the selected local area is possible by not conventional XPS system but 3DnanoESCA. The partially reduced state after Li insertion should have mobile domain-walls that separate the Ti^{4+} and Ti^{3+} sites; however, such a domain-wall was not measured in this experiment. Further experiments will be carried out to provide evidence for the partial reduction of the Ti site by replacing the dry polymer electrolytes with all solid-state LIBs constructed by all ceramics electrolytes to avoid significant contamination derived from Li-F composite by SEI for highly durable and cutting-edge analysis.

4. Conclusions

Reversible changes of the photoelectron spectra of Ti 3*p* of single crystalline $Li_4Ti_5O_{12}$ particles with octahedral-like morphology by Li insertion and extraction were confirmed by microscopic X-ray photoelectron spectroscopy under the potential control of all solid-state LIBs. This *operando* measurement system is a powerful technique to understand the micro-area chemical state of materials for LIBs because this method can analyze various kinds of materials by only changing of the slurry. In future, use of all ceramics solid-state electrolytes will lead to a further detailed understanding of electrode materials of LIBs.

Acknowledgements

This work is partially conducted on the basis of the International joint research program for innovative energy technology by Ministry of Economy, Trade and Industry, Japan. A part of this work was supported by TIA collaborative research program “Kakehashi”, the Research Program for CORE lab of “Five-star Alliance” in “NJRC Mater. & Dev.” and JST, PRESTO Grant Number JPMJPR17NB, Japan. Experiments at SPring-8 BL07LSU were performed jointly by the Synchrotron Radiation Research Organization and the University of Tokyo (proposal nos. 2015B7402, 2016A7402, 2016B7402, 2017A7402, 2017B7402, 2018A7563, 2018A7567).

References

[1] V. Etacheri, R. Marom, R. Elazari, G. Salitra, D. Aurbach, Challenges in the development of advanced Li-ion batteries: a review, Energy Environ. Sci. 4 (2011) 3243–3262, https://doi.org/10.1039/c1ee01598b.

[2] Y.Q. Wang, L. Gu, Y.G. Guo, H. Li, X.Q. He, S. Tsukimoto, Y. Ikuhara, L.J. Wan, Rutile-TiO_2 nanocoating for a high-rate $Li_4Ti_5O_{12}$ anode of a lithium-ion battery, J. Am. Chem. Soc. 134 (2012) 7874–7879, https://doi.org/10.1021/ja301266w.

[3] X. Lu, Y. Sun, Z. Jian, X. He, L. Gu, Y. Hu, H. Li, Z. Wang, W. Chen, X. Duan, L. Chen, J. Maier, S. Tsukimoto, Y. Ikuhara, New insight into the atomic structure of electrochemically delithiated O3-$Li_{(1-x)}CoO_2$ ($0 \le x \le 0.5$) nanoparticles, Nano Lett. 12 (2012) 6192–6197, https://doi.org/10.1021/nl303036e.

[4] D. Asakura, E. Hosono, M. Okubo, Y. Nanba, H. Zhou, P.A. Glans, J. Guo, Correlation between the O 2p orbital and redox reaction in $LiMn_{0.6}Fe_{0.4}PO_4$ nanowires studied by soft x-ray absorption, ChemPhysChem. 17 (2016) 4110–4115, https://doi.org/10.1002/cphc.201600952.

[5] D. Asakura, Y. Nanba, Y. Makinose, H. Matsuda, E. Hosono, Investigation of the relationship between the cycle performance and the electronic structure in $LiAl_xMn_{2-x}O_4$ (x = 0 and 0.2) using soft X-ray spectroscopy, Phys. Chem. Chem. Phys. 19 (2017) 16507–16511, https://doi.org/10.1039/C7CP02070H.

[6] W. Huang, A. Marcelli, D. Xia, Application of synchrotron radiation technologies to electrode materials for Li- and Na-ion batteries, Adv. Energy Mater. 7 (2017) 1700460, , https://doi.org/10.1002/aenm.201700460.

[7] H. Song, T.-G. Jeong, Y.H. Moon, H.-H. Chun, K.Y. Chung, H.S. Kim, B.W. Cho, Y.-T. Kim, Stabilization of oxygen-deficient structure for conducting $Li_4Ti_5O_{12-\delta}$ by molybdenum doping in a reducing atmosphere, Sci. Rep. 4 (2015) 4350, https://doi.org/10.1038/srep04350.

[8] L. Dahéron, R. Dedryvère, H. Martinez, M. Ménétrier, C. Denage, C. Delmas, D. Gonbeau, Electron transfer mechanisms upon Lithium deintercalation from $LiCoO_2$ to CoO investigated by XPS, Chem. Mater. 20 (2008) 583–590, https://doi.org/10.1021/cm70.2546s.

[9] M.-S. Song, R.-H. Kim, S.-W. Baek, K.-S. Lee, K. Park, A. Benayad, Is $Li_4Ti_5O_{12}$ a solid-electrolyte-interphase-free electrode material in Li-ion batteries? Reactivity between the $Li_4Ti_5O_{12}$ electrode and electrolyte, J. Mater. Chem. A 2 (2014) 631–636, https://doi.org/10.1039/C3TA12728A.

[10] J.-W. Park, C.-M. Park, A fundamental understanding of Li insertion/extraction behaviors in SnO and SnO_2, J. Electrochem. Soc. 162 (2015) A2811–A2816, https://doi.org/10.1149/2.0891514jes.

[11] K.T. Kim, C.Y. Yu, C.S. Yoon, S.J. Kim, Y.K. Sun, S.T. Myung, Carbon-coated $Li_4Ti_5O_{12}$ nanowires showing high rate capability as an anode material for rechargeable sodium batteries, Nano Energy 12 (2015) 725–734, https://doi.org/10.1016/j.nanoen.2015.01.034.

[12] S.-M. Bak, Z. Shadike, R. Lin, X. Yu, X.-Q. Yang, In situ/operando synchrotron-based X-ray techniques for lithium-ion battery research, NPG Asia Mater. 10 (2018) 563–580, https://doi.org/10.1038/s41427-018-0056-z.

[13] P.P.R.M.L. Harks, F.M. Mulder, P.H.L. Notten, In situ methods for Li-ion battery research: a review of recent developments, J. Power Sources 288 (2015) 92–105, https://doi.org/10.1016/j.jpowsour.2015.04.084.

[14] H. Wang, F. Wang, *In situ, operando* measurements of rechargeable batteries, Curr. Opin. Chem. Eng. 13 (2016) 170–178, https://doi.org/10.1016/J.COCHE.2016.09.002.

[15] D. Asakura, E. Hosono, H. Niwa, H. Kiuchi, J. Miyawaki, Y. Nanba, M. Okubo, H. Matsuda, H. Zhou, M. Oshima, Y. Harada, *Operando* soft x-ray emission spectroscopy of $LiMn_2O_4$ thin film involving Li-ion extraction/insertion reaction, Electrochem. commun. 50 (2015) 93–96, https://doi.org/10.1016/j.elecom.2014.09.015.

[16] G. Aquilanti, M. Giorgetti, R. Dominko, L. Stievano, I. Arčon, N. Novello, L. Olivi, *Operando* characterization of batteries using x-ray absorption spectroscopy: advances at the beamline XAFS at synchrotron Elettra, J. Phys. D Appl. Phys. 50 (2017) 074001, , https://doi.org/10.1088/1361-6463/aa519a.

[17] N.K. Karan, M.D. Slater, F. Dogan, D. Kim, C.S. Johnson, M. Balasubramanian, Operando structural characterization of the lithium-substituted layered sodium-ion cathode material P2-$Na_{0.85}Li_{0.17}Ni_{0.21}Mn_{0.64}O_2$ by X-ray absorption spectroscopy, J. Electrochem. Soc. 161 (2014) A1107–A1115, https://doi.org/10.1149/2.088406jes.

[18] X. Liu, J. Liu, R. Qiao, Y. Yu, H. Li, L. Suo, Y.S. Hu, Y. De Chuang, G. Shu, F. Chou, T.C. Weng, D. Nordlund, D. Sokaras, Y.J. Wang, H. Lin, B. Barbiellini, A. Bansil, X. Song, Z. Liu, S. Yan, G. Liu, S. Qiao, T.J. Richardson, D. Prendergast, Z. Hussain, F.M.F. De Groot, W. Yang, Phase transformation and lithiation effect on electronic structure of Li_xFePO_4: an in-depth study by soft X-ray and simulations, J. Am. Chem. Soc. 134 (2012) 13708–13715, https://doi.org/10.1021/ja303225e.

[19] X. Liu, D. Wang, G. Liu, V. Srinivasan, Z. Liu, Z. Hussain, W. Yang, Distinct charge dynamics in battery electrodes revealed by *in situ* and *operando* soft X-ray spectroscopy, Nat. Commun. 4 (2013) 2568, https://doi.org/10.1038/ncomms3568.

[20] F. Lin, I.M. Markus, D. Nordlund, T.-C. Weng, M.D. Asta, H.L. Xin, M.M. Doeff, Surface reconstruction and chemical evolution of stoichiometric layered cathode materials for lithium-ion batteries, Nat. Commun. 5 (2014) 3529, https://doi.org/10.1038/ncomms4529.

[21] K. Horiba, Y. Nakamura, N. Nagamura, S. Toyoda, H. Kumigashira, M. Oshima, K. Amemiya, Y. Senba, H. Ohashi, Scanning photoelectron microscope for nanoscale three-dimensional spatial-resolved electron spectroscopy for chemical analysis, Rev. Sci. Instrum. 82 (2011) 113701, , https://doi.org/10.1063/1.3657156.

[22] N. Nagamura, K. Horiba, S. Toyoda, S. Kurosumi, T. Shinohara, M. Oshima, H. Fukidome, M. Suemitsu, K. Nagashio, A. Toriumi, Direct observation of charge transfer region at interfaces in graphene devices, Appl. Phys. Lett. 102 (2013) 241604, , https://doi.org/10.1063/1.4808083.

[23] N. Nagamura, S. Ito, K. Horiba, T. Shinohara, M. Oshima, S. Nishimura, A. Yamada, N. Mizuno, Spectromicroscopic analysis of lithium intercalation in spinel $LiMn_2O_4$ for lithium-ion battery by 3D nano-ESCA, J. Phys. Conf. Ser. 502 (2014) 012013, , https://doi.org/10.1088/1742-6596/502/1/012013.

[24] N. Nagamura, Y. Kitada, J. Tsurumi, H. Matsui, K. Horiba, I. Honma, J. Takeya, M. Oshima, Chemical potential shift in organic field-effect transistors identified by soft X-ray *operando* nano-spectroscopy, Appl. Phys. Lett. 106 (2015) 251604, , https://doi.org/10.1063/1.4922902.

[25] K. Akada, T. Sudayama, D. Asakura, H. Kitaura, N. Nagamura, K. Horiba, M. Oshima, E. Hosono, Y. Harada, Microscopic photoelectron analysis of single crystalline LiCoO2 particles during the charge-discharge in an all solid-state lithium ion battery, (n.d.) Submitt. to Elsewhere.

[26] Q.Q. Liu, D.J. Xiong, R. Petibon, C.Y. Du, J.R. Dahn, Gas evolution during unwanted lithium plating in Li-ion cells with EC-based or EC-free electrolytes, J. Electrochem. Soc. 163 (2016) A3010–A3015, https://doi.org/10.1149/2.0711614jes.

[27] V. Zinth, C. von Lüders, M. Hofmann, J. Hattendorff, I. Buchberger, S. Erhard, J. Rebelo-Kornmeier, A. Jossen, R. Gilles, Lithium plating in lithium-ion batteries at sub-ambient temperatures investigated by in situ neutron diffraction, J. Power Sources 271 (2014) 152–159, https://doi.org/10.1016/J.JPOWSOUR.2014.07.168.

[28] K. Eberman, P. Gomadam, G. Jain, E. Scott, Material and design options for avoiding lithium plating during charging, ECS Trans., The Electrochemical Society (2010) 47–58, https://doi.org/10.1149/1.3414003.

[29] B. Zhao, R. Ran, M. Liu, Z. Shao, A comprehensive review of $Li_4Ti_5O_{12}$-based electrodes for lithium-ion batteries: the latest advancements and future perspectives, Mater. Sci. Eng. R. 98 (2015) 1–71, https://doi.org/10.1016/j.mser.2015.10.001.

[30] N. Nitta, F. Wu, J.T. Lee, G. Yushin, Li-ion battery materials: present and future, Mater. Today. 18 (2015) 252–264, https://doi.org/10.1016/j.mattod.2014.10.040.

[31] H.-G. Jung, M.W. Jang, J. Hassoun, Y.-K. Sun, B. Scrosati, A high-rate long-life $Li_4Ti_5O_{12}$/$Li[Ni_{0.45}Co_{0.1}Mn_{1.45}]O_4$ lithium-ion battery, Nat. Commun. 2 (2011) 516, https://doi.org/10.1038/ncomms1527.

[32] X. Lu, L. Zhao, X. He, R. Xiao, L. Gu, Y.-S. Hu, H. Li, Z. Wang, X. Duan, L. Chen, J. Maier, Y. Ikuhara, Lithium storage in $Li_4Ti_5O_{12}$ spinel: the full static picture from electron microscopy, Adv. Mater. 24 (2012) 3233–3238, https://doi.org/10.1002/adma.201200450.

[33] X. Lu, L. Gu, Y.-S. Hu, H.-C. Chiu, H. Li, G.P. Demopoulos, L. Chen, New insight into the atomic-scale bulk and surface structure evolution of $Li_4Ti_5O_{12}$ anode, J. Am. Chem. Soc. 137 (2015) 1581–1586, https://doi.org/10.1021/ja5115562.

[34] M. Kitta, T. Akita, S. Tanaka, M. Kohyama, Characterization of two phase distribution in electrochemically-lithiated spinel $Li_4Ti_5O_{12}$ secondary particles by electron energy-loss spectroscopy, J. Power Sources 237 (2013) 26–32, https://doi.org/10.1016/j.jpowsour.2013.03.022.

[35] A. Deschanvres, B. Raveau, Z. Sekkal, Mise en evidence et etude cristallographique d'une nouvelle solution solide de type spinelle $Li_{1+x}Ti_{2-x}O_4$ $0 \leqslant x \leqslant 0, 33_3$, Mater. Res. Bull. 6 (1971) 699–704, https://doi.org/10.1016/0025-5408(71)90103-6.

[36] M. Oku, K. Wagatsuma, S. Kohiki, Ti 2p and Ti 3p X-ray photoelectron spectra for TiO_2, $SrTiO_3$ and $BaTiO_3$, Phys. Chem. Chem. Phys. 1 (1999) 5327–5331, https://doi.org/10.1039/a907161j.

[37] J.-B. Gieu, V. Winkler, C. Courrèges, L. El Ouatani, C. Tessier, H. Martinez, New insights into the characterization of the electrode/electrolyte interfaces within $LiMn_2O_4$/$Li_4Ti_5O_{12}$ cells, by X-ray photoelectron spectroscopy, scanning Auger microscopy and time-of-fligh, J. Mater. Chem. A 5 (2017) 15315–15325, https://doi.org/10.1039/C7TA02529G.

[38] M.S. Martín González, M.H. Aguirre, E. Morán, M.Á. Alario-Franco, V. Perez-Dieste, J. Avila, M.C. Asensio, M.S. Martı, M.H. Aguirre, E. Mora, M.C. Asensio, In situ reduction of (100) $SrTiO_3$, Solid State Sci. 2 (2000) 519–524, https://doi.org/10.1016/S1293-2558(00)01068-2.